separations

MDPI

Article

Effect of Internal Vortex-Finder on Classification Performance for Double Vortex-Finder Hydrocyclone

Yuekan Zhang *, Jiangbo Ge, Lanyue Jiang, Hui Wang and Yaoxu Duan

College of Mechanical & Electronic Engineering, Shandong University of Science and Technology, Qingdao 266590, China; gjbsk2808@163.com (J.G.); jianglanyue5@163.com (L.J.); wang_hui_1992@163.com (H.W.); dyx1113611944@163.com (Y.D.)

* Correspondence: zhangyk2007@sdust.edu.cn; Tel.: +86-0532-8605-7176

Abstract: The double vortex-finder hydrocyclone formed by a coaxial insertion of an internal vortex-finder with a smaller diameter inside the conventional single vortex-finder used to obtain two kinds of products from the internal and external overflows in one classification has attracted wide attention. To further improve the classification performance of the hydrocyclone, the effects of the internal vortex-finder diameter and length on the classification performance were studied by numerical simulation and response surface modeling with the behavior of fluid and particle motion in the double vortex-finder hydrocyclone as the research object. The results showed that the split ratio and pressure drop of internal and external overflow increased with the diameter of the internal vortex-finder. The classification performance was optimal when the diameter ratio of internal and external overflow was 0.88, the yield of −20 μm particles was more than 80.0%, and the highest was 95.0%. Increasing the internal vortex-finder length could reduce the coarse particle content and improve the classification accuracy of the internal overflow product. When the length of the internal vortex-finder is larger than 80 mm, the +30 μm yield was lower than 20.0%, and the maximum k value was 16.3%; the k is the significant factor used to characterize the effectiveness of −20 μm particle collection. The response surface modeling revealed that the internal vortex-finder diameter was the most important factor affecting the distribution rate of internal overflow. This paper is expected to advance the development of the classification industry.

Keywords: hydrocyclone; CFD; separation performance; central composite response surface; flow field characteristics

check for updates

Citation: Zhang, Y.; Ge, J.; Jiang, L.; Wang, H.; Duan, Y. Effect of Internal Vortex-Finder on Classification Performance for Double Vortex-Finder Hydrocyclone. *Separations* **2022**, *9*, 88. https://doi.org/10.3390/separations9040088

Academic Editor: Ronald Beckett

Received: 21 February 2022
Accepted: 28 March 2022
Published: 31 March 2022

Publisher's Note: MDPI stays neutral with regard to jurisdictional claims in published maps and institutional affiliations.

Copyright: © 2022 by the authors. Licensee MDPI, Basel, Switzerland. This article is an open access article distributed under the terms and conditions of the Creative Commons Attribution (CC BY) license (https://creativecommons.org/licenses/by/4.0/).

1. Introduction

Hydrocyclone is a piece of simple-structure and efficient solid–liquid classification equipment with a history of more than 100 years [1]. With its excellent classification performance, hydrocyclone is widely used in mineral processing, the chemical industry, petroleum, etc. [2–5]. However, the mismatch phenomenon of coarse particles entrained in the overflow product and fine particles entrained in the bottom flow product has always existed in the hydrocyclone classification process [6,7].

To effectively improve the classification performance of hydrocyclone, researchers have conducted in-depth research on the structure of the vortex-finder to improve the classification efficiency of the hydrocyclone by changing the structure of the vortex-finder. Qiang et al. [8] considered that the diameter of the vortex-finder could significantly affect hydrocyclone classification performance, and the appropriate reduction of the vortex-finder diameter could reduce the cut size. Ghodrat et al. [9,10] considered that the diameter was the most influential element for classification efficiency among the vortex-finder parameters, and a too large or too small vortex-finder diameter could lead to the loss of hydrocyclone classification capacity. Cui et al. [11] consider that an extension of the diameter of the vortex-finder may lead to an outward shift of the zero-axis velocity envelope, resulting in a

coarse overflow. Therefore, the vortex-finder diameter is an extremely valuable indicator affecting the hydrocyclone classification behavior.

The insertion depth of the vortex-finder is an important factor affecting the hydrocyclone classification efficiency and classification accuracy [12–14]. Liu et al. [15] concluded that the most efficient classification was achieved when the insertion depth of the vortex-finder was at the column–cone junction of the hydrocyclone. Hwang et al. [10,16] believed that with the increase in the insertion depth of the overflow pipe, the separation efficiency showed a trend of increasing first and then decreasing. Tian et al. [17] found through numerical simulation that the optimal length of overflow pipe should be 1.682.02 times of column length. Therefore, the vortex-finder length is crucial to the hydrocyclone classification efficiency. However, no unified qualitative conclusion has been obtained from many in-depth studies on the vortex-finder length.

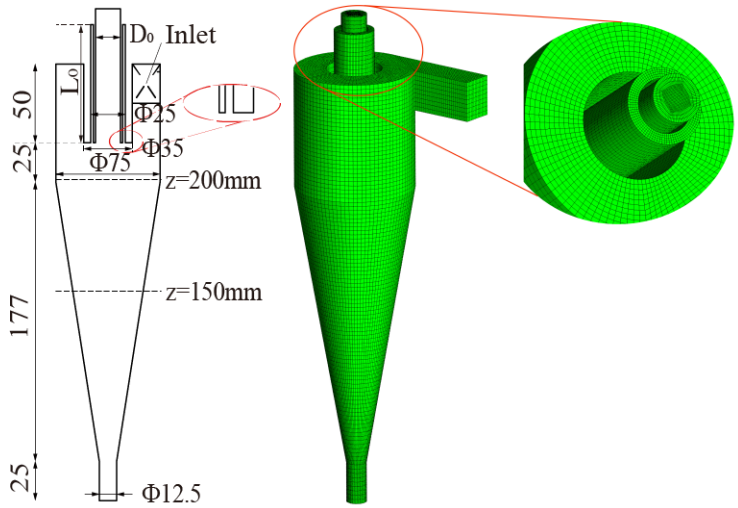
In addition to numerical simulation methods, multi-factor experimental design has become an important means to study the influence of structural parameters on the hydrocyclone separation effect. The comprehensive influence of multiple structural factors on hydrocyclone classification efficiency was investigated using the response surface method and orthogonal experiments to seek the optimal structural size of hydrocyclone [18–20]. Tang et al. [10] studied the influence rules of the overflow tube diameter, insertion depth, and wall thickness on the classification efficiency of the cyclone by response surface method, and found that the overflow tube diameter was the most important factor affecting the classification efficiency. Liu et al. [15] found the comprehensive influence relationship of inlet flow rate, vortex-finder insertion depth, and vortex-finder wall thickness on hydrocyclone classification efficiency using orthogonal experiments.

To obtain two kinds of products from the internal and external overflows in one classification, Obeng et al. [21,22] designed a double vortex-finder hydrocyclone, a coaxial insertion of a smaller internal vortex-finder inside the conventional single vortex-finder, which received wide attention. However, the influence of structural parameters of dual overflow pipe on flow field and separation efficiency is not clear. The influence of the internal vortex-finder diameter and length on the hydrocyclone flow field was analyzed by numerical simulation to explore the influence of the structural parameters of the double vortex-finder hydrocyclone on the classification. The response surface model of the internal vortex-finder diameter, length, and classification accuracy was established by the central composite response surface method to improve the classification performance of the double vortex-finder hydrocyclone. This paper can advance the development of the classification industry.

2. Model and Validation

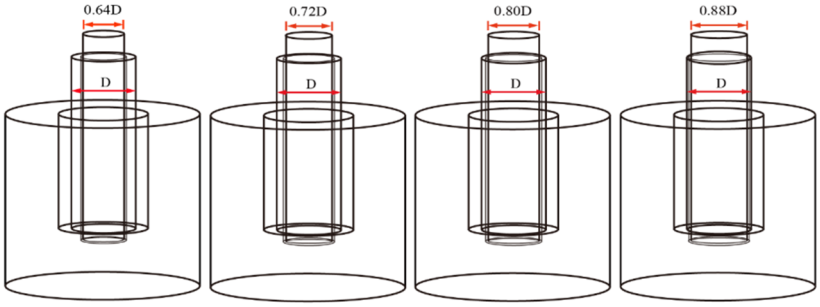
2.1. Hydrocyclone Structure and Grid Division

The double vortex-finder hydrocyclone in this paper is evolved from the Φ75 conventional hydrocyclone by adding an internal overflow pipe. The structure diagram is shown in Figure 1a. D_0 is the internal overflow pipe diameter, and L_0 is the insertion depth of the internal overflow pipe. To facilitate the study of the influence law of overflow, the overflow pipe structure parameters on the hydrocyclone flow field, and classification efficiency, the ratio of vortex-finder diameter, insertion depth, and the corresponding parameters of cone section in the hydrocyclone are often studied as dimensionless factors [23–25]. Therefore, the ratio of the internal overflow pipe diameter D_0 to the external D and the ratio of the internal overflow pipe insertion depth L_0 to the external L were regarded as the influencing factors on flow distribution and investigated in study. When D_0 = (0.64–0.88) D, the internal vortex-finder is 80 mm, as shown in Figure 2. When L_0 = (0.86–1.26) L, the internal vortex-finder diameter is 20 mm, as shown in Figure 3.



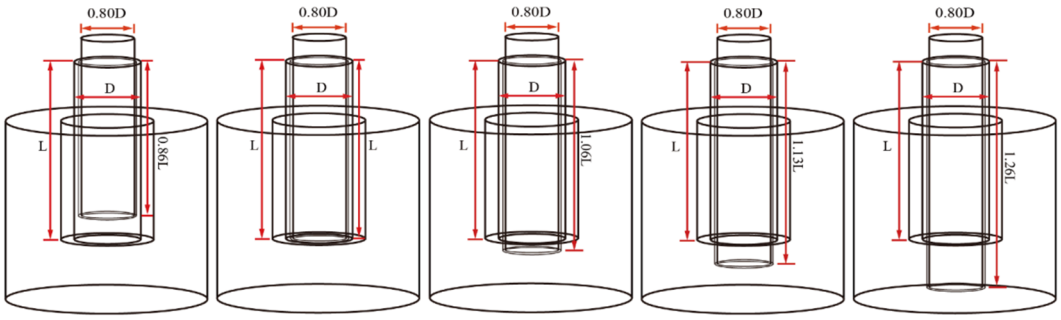
(**a**) (**b**)

Figure 1. Hydrocyclone construction and meshing diagram. (**a**) Structure diagram. (**b**) Mesh.



(**a**) (**b**) (**c**) (**d**)

Figure 2. Double vortex-finder hydrocyclone in different diameter configurations. (**a**) 0.64 D (**b**) 0.72 D (**c**) 0.80 D (**d**) 0.88 D.



(**a**) (**b**) (**c**) (**d**) (**e**)

Figure 3. Double vortex-finder hydrocyclone in different length configurations. (**a**) 0.86 L (**b**) 1.00 L (**c**) 1.06 L (**d**) 1.13 L (**e**) 1.26 L.

The double vortex-finder hydrocyclone fluid domain is meshed using ICEM18.0 software, as shown in Figure 1b. To verify the irrelevance of the grid, the tangential velocity with different grid numbers of 150,000, 250,000, 300,000, and 400,000 are measured, as shown in Figure 4. The results show that the tangential velocity is the same when the mesh number is greater than 300,000, revealing the irrelevance of the grid. The grid number

of the hydrocyclone fluid domain is determined to be 300,000 in consideration of the computational cost and simulation accuracy.

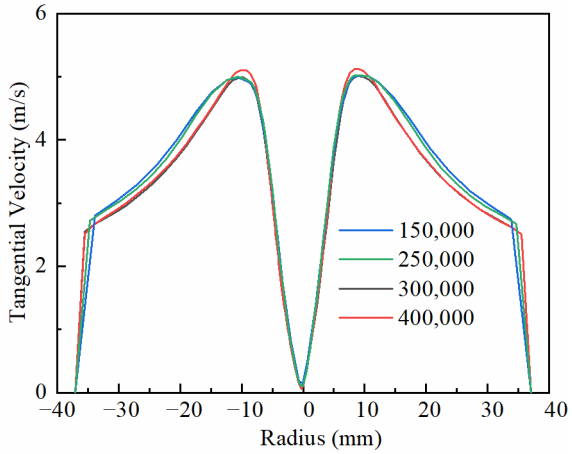


Figure 4. Verification of grid independence.

2.2. Mathematical Model

The accuracy of the VOF model for predicting the clear water field in the hydrocyclone has been verified, and the model achieves the capture of the air core section by solving the momentum equation (Equation (1)) to predict the flow field characteristics [26,27].

$$\frac{\partial \alpha_q}{\partial t} + v_j \frac{\partial \alpha_q}{\partial x_j} = 0 \tag{1}$$

where α_q is the volume fraction of the q phase, v_j is the velocity in the j direction of the q phase, and t and x_j represent the time and length of the position, respectively.

The Mixture model can efficiently accomplish low concentration discrete phase classification prediction by calculating the mixed term momentum equation (Equation (2)) and the continuity equation (Equation (3)) [28,29].

$$\frac{\partial}{\partial t}(\rho_m) + \nabla\left(\rho_m \vec{v_m}\right) = 0 \tag{2}$$

$$\frac{\partial}{\partial t}(\rho_m) + \nabla\left(\rho_m \vec{v_m} \vec{v_m}\right) = -\nabla p + \nabla \cdot \left[\mu_m \left(\nabla \vec{v_m} + \nabla \vec{v}_m^T\right)\right] + \rho_m \vec{g} + \vec{F} - \nabla \cdot \left(\sum_{k=1}^{n} \alpha_k \rho_k \vec{v}_{dr,k} \vec{v}_{dr,k}\right) \tag{3}$$

where ρ_m is the density of the phases being mixed, v_m is the average mixed-phase velocity, p is the pressure, g is the gravitational force, F is the bulk force, and $\alpha_k \rho_k$ is the k phase viscosity, and $v_{dr,k}$ is the k phase drift velocity.

The RSM model meets the prediction of the complex flow field in the hydrocyclone, considering the various anisotropy assumptions in the turbulent flow field [30–32], and is solved by the transport equation (Equation (4)).

$$\frac{\partial}{\partial t}\left(\rho \overline{\mu_i' \mu_j'}\right) + \frac{\partial}{\partial x_k}\left(\rho \mu_k \overline{\mu_i' \mu_j'}\right) = -D_{\tau,ij} + D_{L,ij} - P_{ij} - G_{ij} + \varphi_{ij} - \varepsilon_{ij} \tag{4}$$

where $\rho \mu_i^{'} \mu_j^{'}$ is the mean Reynolds stress, $D_{\tau,ij}$ is the turbulent diffusion, $D_{L,ij}$ is the molecular diffusion, p_{ij} is the pressure, G_{ij} is the generation, φ_{ij} is the pressure strain term, ε_{ij} is the dissipation, ρ is the fluid density, and μ_k is the fluid viscosity.

2.3. Model Parameters

The RSM model was adopted for the turbulence model, the VOF model and the Mixture model were adopted for the multiphase flow model. The entrance was set to

Velocity-inlet, and the exit was set to Pressure-out. SIMPLE was adopted for pressure-velocity coupling, PRESTO was adopted for pressure discretization, and QUICK format was adopted for other discretization methods. The inlet velocity was 2.28 m/s, the reflux coefficient was 1, and the initial pressure of the flow field was 1 standard atmosphere. $CaCO_3$ particles with a volume fraction of 5.4% are adopted for the dispersion phase, and the particle properties are seen in Table 1. The flow imbalance error of each phase in unit time is less than 5×10^{-3} s as the basis for the convergence of the calculation.

Table 1. Particle properties.

Size/μm	Value of Simulation/μm	Fraction Finer Than Size/%
−5	2.50	6.48
5~10	7.50	17.96
10~15	12.50	31.85
15~25	20.00	57.41
25~35	30.00	75.93
35~45	40.00	89.81
45~55	50.00	96.21
55~60	57.50	100.00

2.4. Model Validation

To verify the accuracy and reliability of the model, the VOF coupled with the RSM model was applied to predict the flow field inside the hydrocyclone. The predicted tangential velocity of the flow field is compared with data measured by Hsieh [33], as can be seen in Figure 5a. The results show the tangential velocity is basically the same, verifying the accuracy of the VOF model. The results of the classification experiments of $CaCO_3$ particles are compared with the prediction of the Mixture model, as shown in Figure 5b. The results show a high consistency, indicating that the Mixture multiphase flow model meets the calculation requirements.

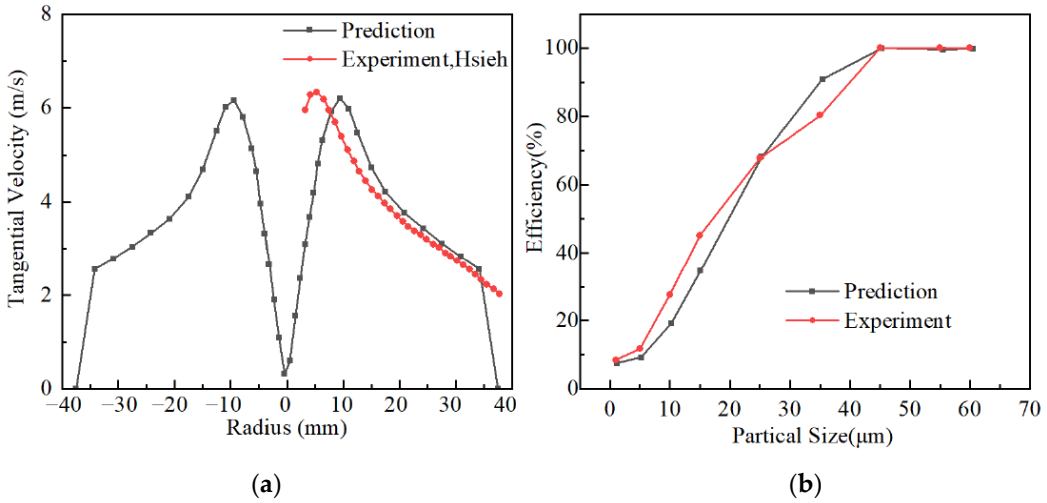


Figure 5. Validation data for the mathematical modeling. (**a**) Validation of VOF (**b**) Validation of Mixture.

2.5. Central Composite Response Surface Design

The optimal parameters of the study factors and significant factors were found in response surface analysis by fitting with multiple quadratic regression equations [34]. The central composite response design was one of the most commonly used response surface design methods [35], widely used in various multi-factor experiments. The comprehensive effect of the interaction of multiple structural factors on hydrocyclone classification efficiency was investigated using the response surface design method. The internal overflow pipe diameter D_0 and insertion depth L_0 were response factors. The optimized value of

steepness index K was chosen as the significant factor to effectively predict the effectively of the internal overflow pipe structure parameters on the classification efficiency of microfine particles with 20 μm in particle size and below, which is calculated as equation (Equation (5)). The design factor levels of the response surface are shown in Table 2.

$$K = (d_{20} - d_{30})/2 \quad (5)$$

where d_{20}, d_{30} are the classification rate of the corresponding particle size.

Table 2. Response surface design levels.

Symbol	Low Levels	High Levels
D_0	0.64 D	0.88 D
L_0	0.86 L	1.26 L

3. Results and Discussion

3.1. Impact of the Internal Vortex-Finder Diameter on the Flow Field

3.1.1. Radial Pressure

Figure 6 shows the diagram of the radial pressure at column and cone sections of the hydrocyclone with different diameters of internal vortex-finder. The variations in diameter have no significant impact on the radial pressure distribution in the flow field at the column section location (z = 200 mm). However, the radial pressure increases with the diameter at the cone section position near the wall area (z = 150 mm). Therefore, the increase in diameter can improve the radial force of the fluid near the wall of the cone section and strengthen the radial motion of the fluid, which is conducive to the particle classification.

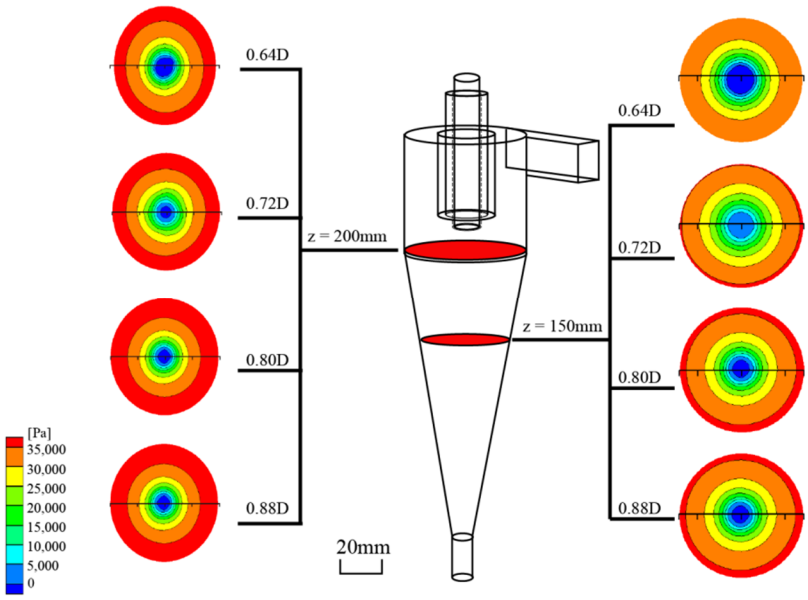


Figure 6. Influence of internal vortex-finder diameter on radial pressure.

3.1.2. Tangential Velocity

Tangential velocity affects the hydrocyclone classification performance. Figure 7 shows distribution curves of the tangential velocity of the double vortex-finder hydrocyclone at different heights. At z = 150 mm and z = 200 mm, within the diameter of 040 mm, the peak tangential velocity is maximum when the diameter is 0.64 D, and the peak tangential velocity is minimum when the diameter is 0.88 D. Within the diameter of 4075 mm, no evident difference in the tangential velocities shows that the tangential velocities are affected by the internal vortex-finder diameter. There are mainly microfine particles within

the diameter of 040 mm and coarse particles within the diameter of 4075 mm. The internal vortex-finder diameter has no significantly effect on coarse particles, but internal vortex-finders with smaller diameters are beneficial to the classification of microfine particles. Accordingly, the internal vortex-finder diameter can be designed according to particle size distribution characteristics of raw materials and the expected classification.

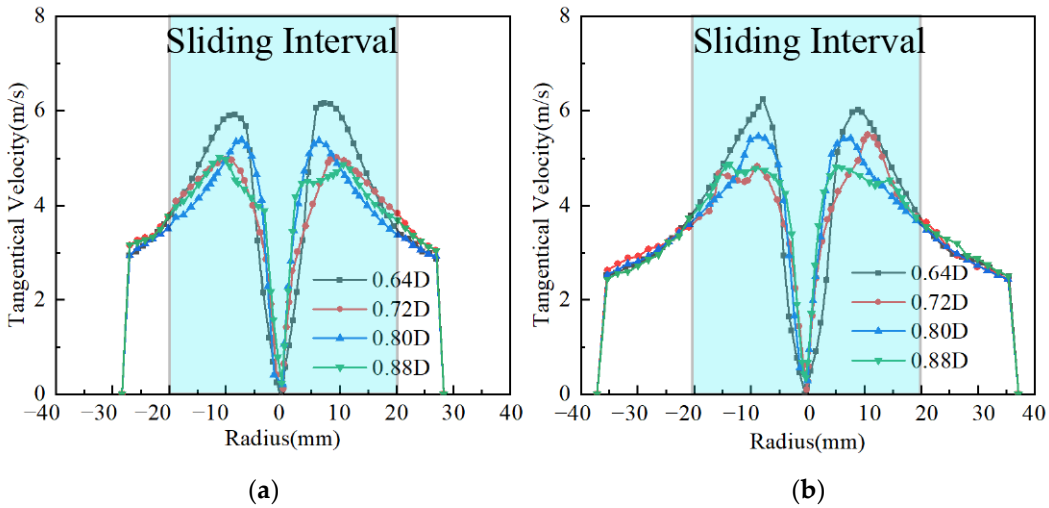


Figure 7. Influence of internal overflow pipe diameter on tangential velocity. (**a**) z = 150 mm (**b**) z = 200 mm.

3.1.3. Air Core

The shape of the air core affects the stability of the flow field. The air core morphology is displayed in Figure 8. The air core diameters all fluctuate between 2 and 6 mm. The diameters of air core increase significantly at the axial position of about 225 mm, forming a protrusion because the air from the overflow and underflow ports meets here and is restricted by the vortex-finder wall. The air core diameter is most stable when diameter D_0 of the internal vortex-finder is 0.72 D, indicating that too large or too small internal vortex-finder diameter will cause the air core to shake violently and is not beneficial to the stabilization of the flow field, thus the internal vortex-finder diameter should be considered in the design of hydrocyclone.

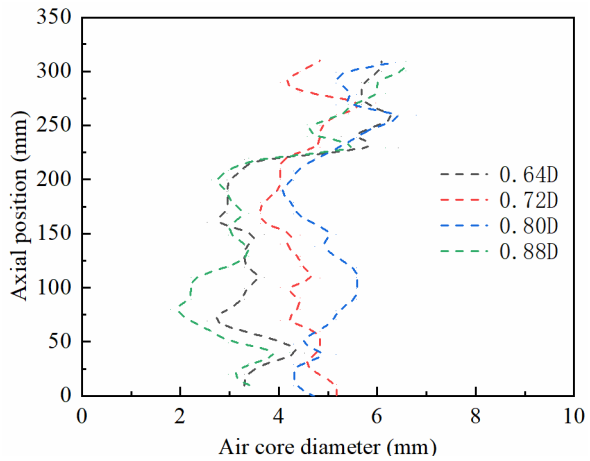


Figure 8. Boundary curve of air core.

3.1.4. Pressure Drop and the Split Ratio of Internal and External Overflow

Figure 9 illustrates the impact of internal overflow pipe diameter pressure drop and the split ratio of internal and external overflow. The pressure drop of the flow field increases

with the internal overflow pipe diameter. Since a large pressure drop means a large energy consumption, the energy consumption in the flow field increases with the internal overflow pipe diameter. Moreover, the increase in the internal overflow pipe diameter increases the split ratio of internal and external overflow. The split ratio of internal and external overflow is only 0.185 when the internal overflow pipe diameter is 16 mm (0.64 D) and up to 1.40 when the internal overflow pipe diameter is 20 mm (0.80 D). When the overflow pipe diameter is small, most of its space is occupied by the air core, causing the split ratio of internal and external overflow to increase rapidly as the internal overflow pipe diameter increases. Therefore, when the internal overflow pipe diameter is less than a certain value, its internal area will be occupied by air, and no product will be separated. In addition, an appropriate increase in the internal overflow pipe diameter will facilitate the overflow of microfine particles from the internal overflow pipe, improving the yield of microfine particles. To better reflect the response of the internal vortex-finder diameter change on the split ratio and pressure drop, the data in the figure was fitted to provide a reference for predicting the distribution of pressure drop and the split ratio of internal and external overflow in internal overflow pipes with different diameters.

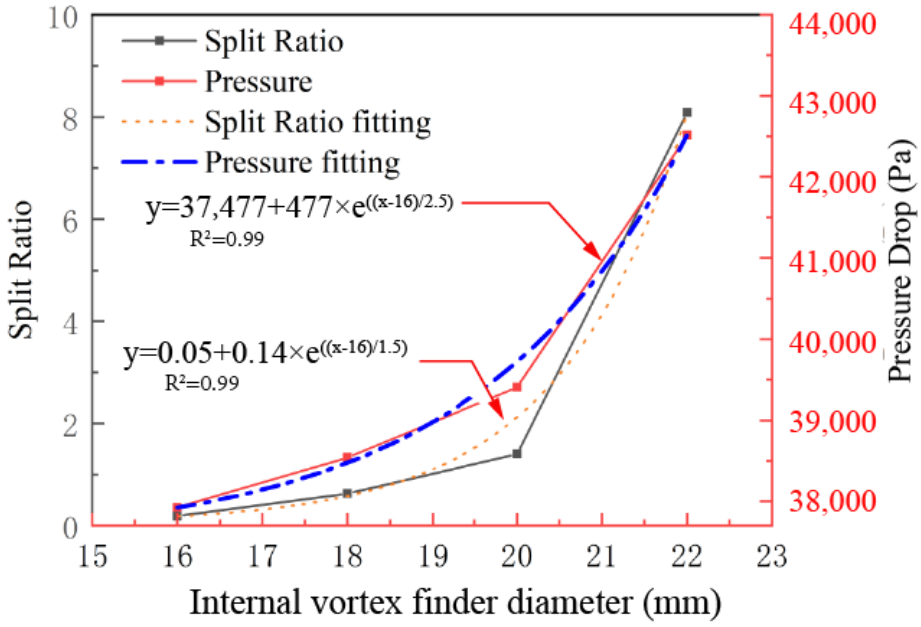


Figure 9. The impact of internal vortex-finder diameter on pressure drop and split ratio.

3.1.5. Pulp Movement Trajectory

Figure 10 shows the pulp movement trajectory of hydrocyclone column section. Due to the internal vortex-finder, most of the short-circuit flow at the hydrocyclone wall (red box in Figure 10) flows into the external overflow area, reducing the total amount of short-circuit flow inside the internal vortex-finder. The classification accuracy is reduced due to the short-circuit flow is directly discharged without effective centrifugal classification. Therefore, the internal overflow pipe with a smaller diameter contributes to the fine classification of internal overflow. However, more pulp in the internal overflow pipe with smaller diameter overflows to the outside, reducing the accuracy of the external overflow.

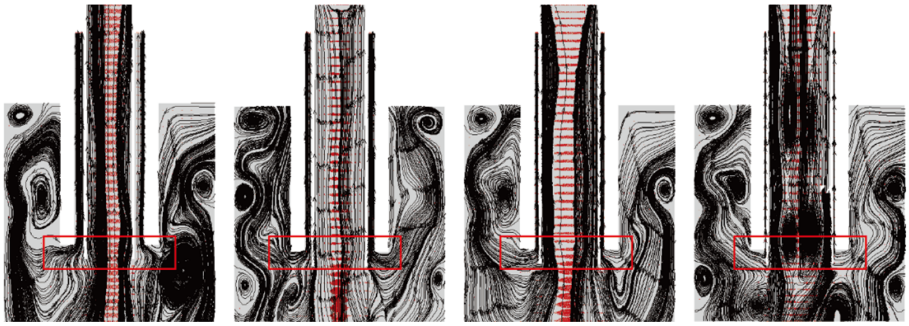


Figure 10. The movement track of liquid under different internal vortex-finder diameters. (**a**) 0.64 D (**b**) 0.72 D (**c**) 0.80 D (**d**) 0.88 D.

3.2. Impact of the Insertion Depth of the Internal Vortex-Finder on the Flow Field

3.2.1. Statistic Pressure Distribution

Figure 11 shows the static pressure distribution of the hydrocyclone. It can be found that the change of the length of the internal overflow pipe has the same effect on the pressure field at different heights. Meanwhile, at a certain height, the radial pressure gradient of the flow field is larger when the internal overflow pipe length is less than or equal to the external overflow pipe length, and the pressure gradient reaches the maximum when the insertion depth of the internal and external vortex finders is the same. Since the direction of the pressure gradient is from the high-pressure area to the low-pressure area, a larger pressure gradient is favorable for the migration of fine particles from the wall to the axis. Thus, when the internal overflow pipe length is less than or equal to the external overflow pipe length, the content of fine particles in the external hydrocyclone region will decrease, improving the classification accuracy of the hydrocyclone.

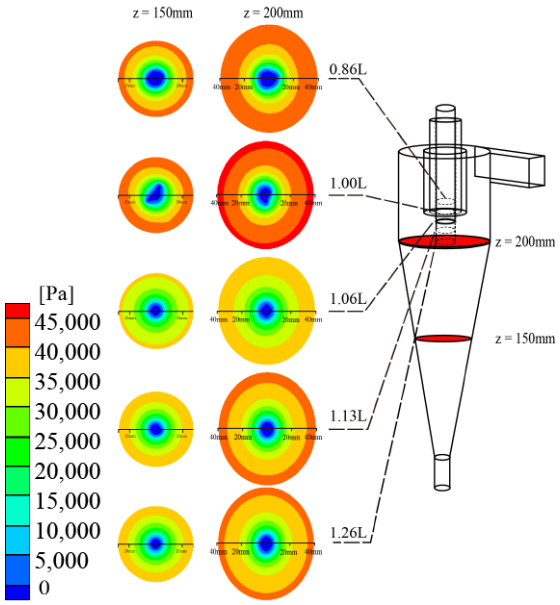
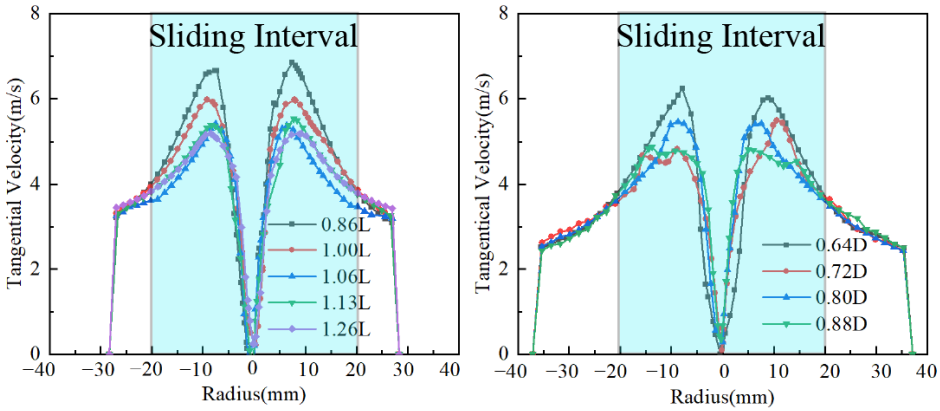


Figure 11. Influence of the insertion depth of the internal overflow pipe on the pressure.

3.2.2. Tangential Velocity

Figure 12 shows the influence of insertion depth of the internal overflow pipe on tangential velocity. Internal overflow pipe length is 0.86 L, tangential velocity variation is concentrated in the range from −20 mm to 20 mm of hydrocyclone radius, and the tangential velocity reaches the maximum. When the internal overflow pipe length is equal to or huger than the outside, the tangential velocity variation decreases gradually. It can be

concluded that the change of the internal overflow pipe length does not significantly affect the centrifugal field of the hydrocyclone when the internal overflow pipe length is equal to or greater than the external overflow pipe.



(**a**) (**b**)

Figure 12. Influence of insertion depth of the internal vortex finder on tangential velocity. (**a**) z = 150 mm (**b**) z = 200 mm.

3.2.3. Pressure Drop and the Split Ratio of Internal and External Overflow

Figure 13 shows the influence of internal overflow pipe length on the hydrocyclone pressure drop and the split ratio of internal and external overflow. The split ratio of internal and external overflow varies from 1.2 to 1.45 with internal vortex-finder lengths. When the insertion depths of internal and external overflow are the same, the split ratio is the largest. Furthermore, the pressure drop is the largest when the insertion depths of the internal and external vortex-finders are the same, indicating that the flush internal and external vortex-finders improve the classification of the flow field. The peak values of pressure drop and the split ratio of internal and external overflow were predicted with data fitting. The results show that the peak pressure drop and peak split ratio correspond to the same internal vortex-finder length, which provides a reference to optimize parameters of the internal vortex-finder insertion length.

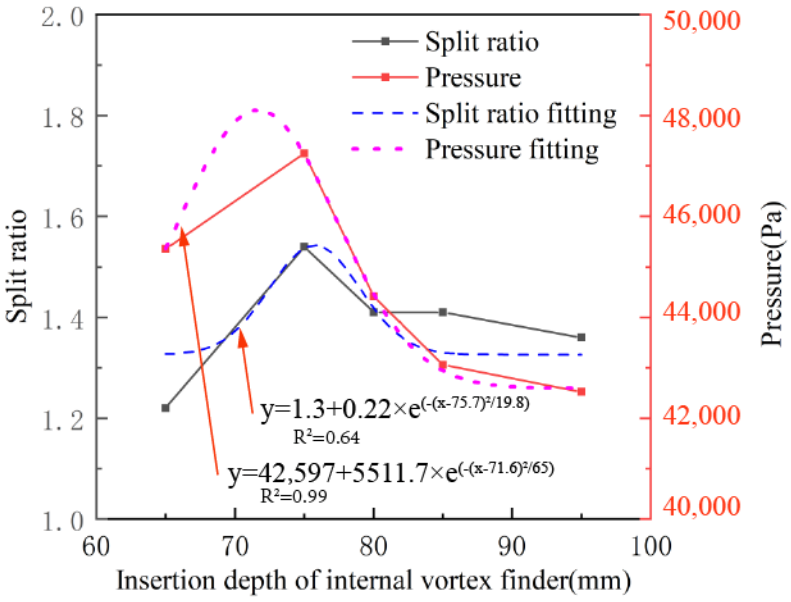
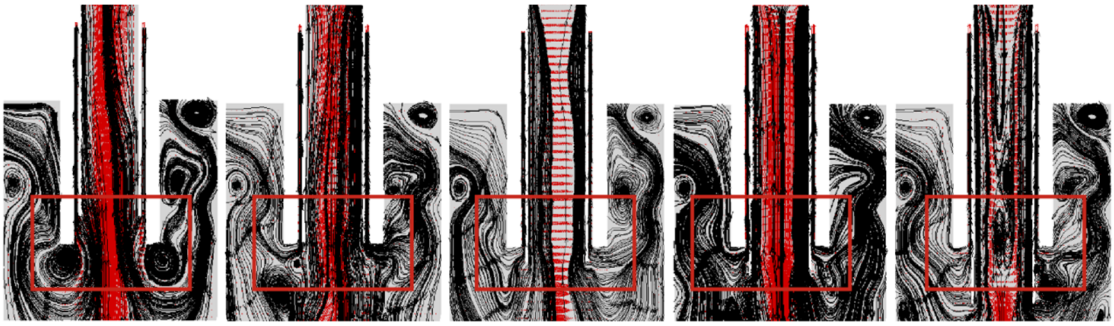


Figure 13. Influence of the insertion depth of the internal vortex finder on pressure drop and split ratio.

3.2.4. Pulp Movement Trajectory

Figure 14 shows the pulp movement trajectory of the hydrocyclone column section with different internal overflow pipe lengths. The axial movement distance of the fluid entering the internal vortex finder gradually increases with the internal overflow pipe length, which is conducive to the residence of the particles in the cyclone field and for particle classification. Meanwhile, the internal overflow pipe length is smaller than the external overflow pipe length, and the vortex is easily formed at the bottom of the vortex-finder, which is not conducive to the stability of the flow field or for the classification accuracy.



(**a**) (**b**) (**c**) (**d**) (**e**)

Figure 14. Slurry movement trajectory of hydrocyclone under different length of internal vortex finder. (**a**) 0.86 L (**b**) 1.00 L (**c**) 1.06 L (**d**) 1.13 L (**e**) 1.26 L.

3.3. Response Surface Model

3.3.1. Model Design

To further explore the influence of internal overflow pipe diameter and insertion depth on the classification efficiency of the cyclone, an optimization model was established according to the central composite design and response surface methodology, as shown in Table 3.

Table 3. Numerical simulation design of central composite response surface.

Test No.	L_0	D_0	K
1	18.00	65.00	6.01
2	22.00	65.00	11.22
3	18.00	95.00	9.58
4	22.00	95.00	16.30
5	17.17	80.00	3.92
6	22.83	80.00	12.87
7	20.00	58.79	7.83
8	20.00	101.21	14.74
9	20.00	80.00	14.00
10	20.00	80.00	14.00
11	20.00	80.00	14.00
12	20.00	80.00	14.00
13	20.00	80.00	14.00

Figure 15 shows the internal overflow rates of hydrocyclones with relevant response surfaces. Figure 15a–i correspond to the first nine combinations in Table 3, respectively. When the internal overflow pipe diameter is small, the classification efficiency of particles with the particle size of 20 μm and below is low, only around 30%, as shown in Figure 15a,c,e. When the internal overflow pipe diameter is large, the corresponding microfine particle classification efficiency can reach over 80%, as shown in Figure 15b,d,f. It should be noted that although increasing the diameter of internal overflow is beneficial to increase the classification efficiency of fine particles, some coarse particles will also be included in the fine particles, reducing the classification accuracy.

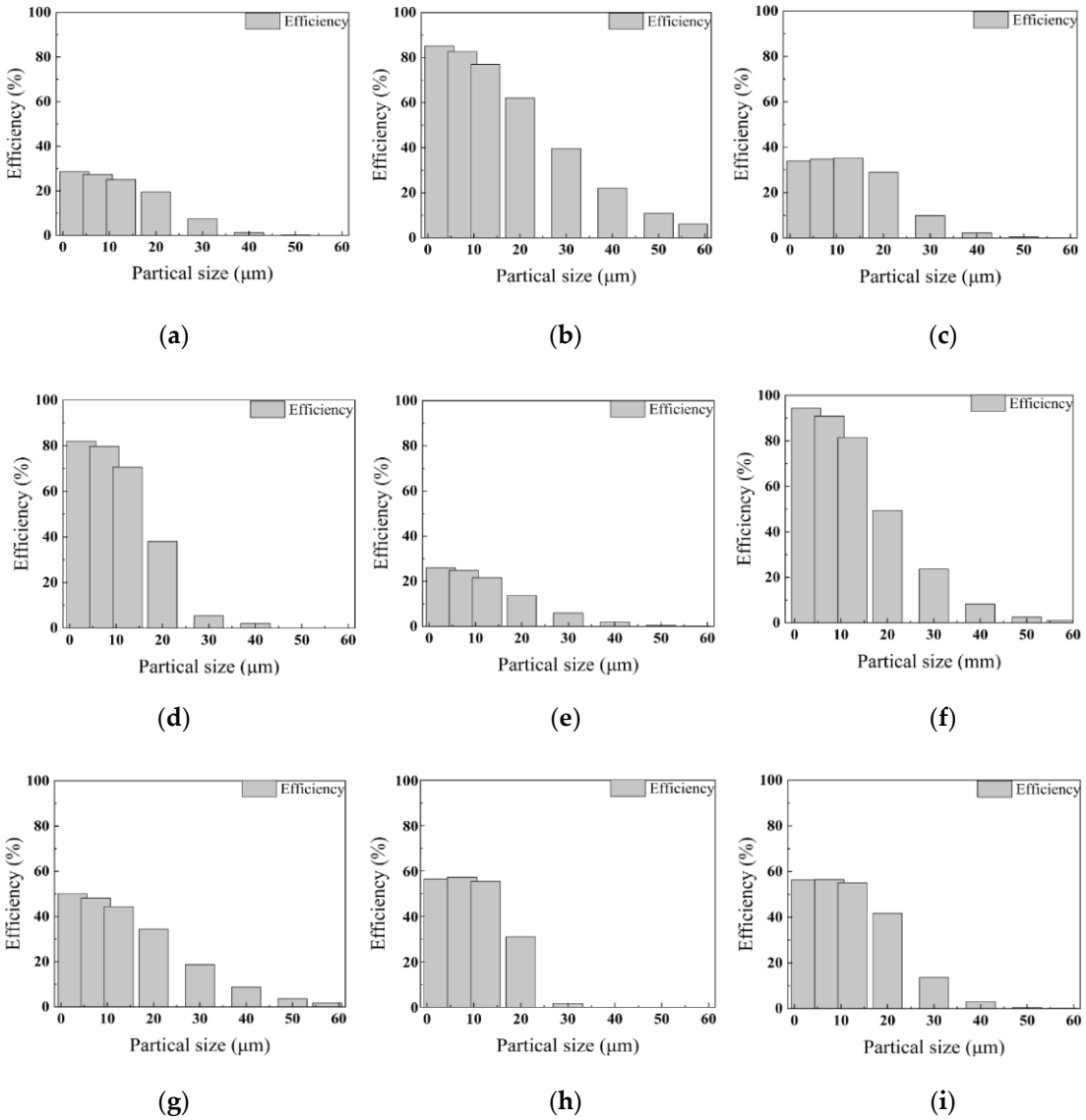


Figure 15. Internal overflow classification efficiency. (**a**) Test 1 (**b**) Test 2 (**c**) Test 3 (**d**) Test 4 (**e**) Test 5 (**f**) Test 6 (**g**) Test 7 (**h**) Test 8 (**i**) Test 9.

3.3.2. Optimization Model Validation

The response function obtained by the quadratic regression equation is as follows.

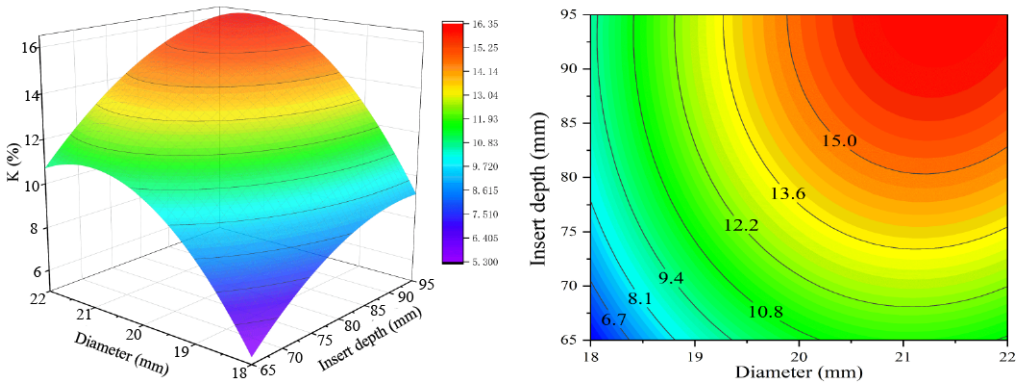
$$K = -297.53 + 26.20 \times D_0 + 0.70 \times L_0 + 0.01 \times D_0 \times L_0 - 0.64 \times D_0^2 - 0.005 \times L_0^2 \quad (6)$$

Analysis of variance and tests need to be performed on the fitted equations for accuracy and reliability [36], and the results are shown in Table 4. To some extent, *p*-value provides the reliability basis for our model [37,38]. The high significance indicates that the fitted regression equation meets the prediction requirements.

Table 4. Error analysis.

Sources	Adjusted Sums of Squares (SS)	Degree of Freedom (DF)	Adjusted Means Squares (MS)	F-Value	*p*-Value
Model	168.89	5.00	33.78	118.81	<0.0001
D_0	75.59	1.00	75.59	265.90	<0.0001
L_0	42.47	1.00	42.47	149.39	<0.0001
$D_0 \times L_0$	0.57	1.00	0.57	2.02	0.1986
$D_0 \times D_0$	45.86	1.00	45.86	161.32	<0.0001
$L_0 \times L_0$	8.76	1.00	8.76	30.83	0.0009

The influence of the internal overflow pipe diameter and insertion depth on the K value is obtained with the central composite response surface optimization. As shown in Figure 16, when the internal overflow pipe diameter is small, despite the change of the insertion depth, the K value is less than 10%. When the internal overflow pipe diameter is large, the K value is above 12%. Therefore, the classification efficiency of the internal overflow pipe in the hydrocyclone increases with the internal overflow pipe diameter. Meanwhile, when the internal overflow pipe diameter is large, the interaction between the internal overflow pipe diameter and the internal overflow pipe insertion depth becomes obvious. The efficiency and accuracy of classification can remain high with an appropriate increase in the internal overflow pipe diameter and a reduction of the internal overflow pipe insertion depth.



(**a**) (**b**)

Figure 16. Response surface diagram. (**a**) Three-dimensional response diagram (**b**) Response surface relationship contour map.

4. Conclusions

With the numerical simulation of the double vortex-finder hydrocyclone and the optimized response surface model of the internal vortex-finder diameter and insertion depth, the following conclusions are drawn.

(1) The flow field pressure drop and split ratio increase with the internal vortex-finder diameter in the double overflow pipe hydrocyclone. The increase in internal overflow pipe length will intensify the flow field fluctuation, and when the internal and external vortex-finder lengths are equal, the flow field pressure drop and split ratio reach the maximum.

(2) The content of fine particles of the internal overflow is positively related to the internal overflow pipe diameter. However, when the ratio of internal and external overflow pipe diameters is over 0.88, the coarse particles in the internal overflow will increase rapidly, reducing the classification accuracy. Moreover, the coarse particle content in the internal overflow pipe gradually decreases with the increase in the insertion depth of the internal overflow pipe.

(3) According to the response surface analysis, when the ratio of internal and external overflow pipe diameters is in the range from 0.8 to 0.88, the interaction between the internal

overflow pipe diameter and insertion depth on classification efficiency is obvious. An appropriate increase in the internal overflow pipe diameter and insertion depth improves the efficiency and accuracy of classification.

In this study, the effects of the internal overflow pipe diameter and insertion depth on the flow field and classification performance have been analyzed. However, the effect of the acting force of particles was ignored in the numerical simulations, which needs to be further studied.

Author Contributions: Conceptualization, Y.Z.; Methodology, Y.Z. and L.J.; Software, J.G. and H.W.; Validation, J.G. and H.W.; Formal Analysis, J.G. and L.J; Investigation, Y.Z. and Y.D.; Resources, Y.D. and L.J.; Writing—Original Draft Preparation, Y.Z.; Writing—Review and Editing, J.G. and L.J. All authors have read and agreed to the published version of the manuscript.

Funding: This research was funded by the Natural Science Foundation of Shandong Province, China (ZR2020ME105), the National Natural Science Foundation of China (22108159), and the Natural Science Foundation of Shandong province, China (ZR2021QB068).

Institutional Review Board Statement: Not applicable.

Informed Consent Statement: Not applicable.

Data Availability Statement: Not applicable.

Conflicts of Interest: The authors declare no conflict of interest.

References

1. Tian, J.; Ni, L.; Song, T.; Shen, C.; Yao, Y.; Zhao, J.N. Numerical study of foulant-water separation using hydrocyclones enhanced by reflux device: Effect of underflow pipe diameter. *Sep. Purif. Technol.* **2019**, *215*, 10–24. [CrossRef]
2. Suresh, P.D.; Kumar, V.; Sripriya, R.; Chakraborty, S.; Meikap, B.C. Performance characteristics of pilot plant dense media hydrocyclone for beneficiation of coal and 3D CFD simulation. *Chem. Eng. Sci.* **2010**, *65*, 4661–4671. [CrossRef]
3. Xie, H.Y.; Sun, R.; Ren, X.J.; You, Z.C.; Liu, Y.H.; Feng, D.X.; Chen, L.Z. Development of a novel fluidized hydrocyclone concentrator for mineral separation. *Sep. Purif. Technol.* **2020**, *248*, 116960. [CrossRef]
4. Li, S.; Li, R.N.; Nicolleau, F.C.G.A.; Wang, Z.C.; Yan, Y.J.; Xu, Y.; Chen, X. Study on oil–water two phase flow characteristics of the hydrocyclone under periodic excitation. *Chem. Eng. Res. Des.* **2020**, *159*, 215–224. [CrossRef]
5. Kyriakidis, Y.N.; Silva, D.O.L.; Barrozo, M.A.S.; Vieira, L.G.M. Effect of variables related to the separation performance of a hydrocyclone with unprecedented geometric relationships. *Powder Technol.* **2018**, *338*, 645–653. [CrossRef]
6. Padhi, M.; Mangadoddy, N.; Sreenivas, T.; Vakamalla, T.R.; Mainza, A.N. Study on multi-component particle behaviour in a hydrocyclone classifier using experimental and computational fluid dynamics techniques. *Sep. Purif. Technol.* **2019**, *229*, 115698. [CrossRef]
7. Ghodrat, M.; Qi, Z.; Kuang, S.B.; Ji, L.; Yu, A.B. Computational investigation of the effect of particle density on the multiphase flows and performance of hydrocyclone. *Miner. Eng.* **2016**, *90*, 55–69. [CrossRef]
8. Yang, O.; Wang, H.L.; Wang, J.G.; Li, Z.M.; Liu, Y. The coordinated relationship between vortex finder parameters and performance of hydrocyclones for separating light dispersed phase. *Sep. Purif. Technol.* **2011**, *79*, 310–320. [CrossRef]
9. Ghodrat, M.; Kuang, S.B.; Yu, A.B.; Vince, A.; Barnett, G.D.; Barnett, P.J. Numerical analysis of hydrocyclones with different vortex finder configurations. *Miner. Eng.* **2014**, *63*, 125–138. [CrossRef]
10. Tang, B.; Xu, Y.X.; Song, X.F.; Sun, Z.; Yu, J.G. Numerical study on the relationship between high sharpness and configurations of the vortex finder of a hydrocyclone by central composite design. *Chem. Eng. J.* **2015**, *278*, 504–516. [CrossRef]
11. Cui, B.Y.; Zhang, C.E.; Wei, D.Z.; Lu, S.S.; Feng, Y.Q. Effects of feed size distribution on separation performance of hydrocyclones with different vortex finder diameters. *Powder Technol.* **2017**, *322*, 114–123. [CrossRef]
12. Martinez, L.F.; Lavin, A.G.; Mahamud, M.M.; Bueno, J.L. Vortex finder optimum length in hydrocyclone Separation. *Chem. Eng. Process. Process Intensif.* **2008**, *47*, 192–199. [CrossRef]
13. Wang, B.; Yu, A.B. Numerical study of the gas–liquid–solid flow in hydrocyclones with different configuration of vortex finder. *Chem. Eng. J.* **2008**, *135*, 33–42. [CrossRef]
14. Silva, N.K.G.; Silva, D.O.; Vieira, L.G.M.; Barrozo, M.A.S. Effects of underflow diameter and vortex finder length on the performance of a newly designed filtering hydrocyclone. *Powder Technol.* **2015**, *286*, 305–310. [CrossRef]
15. Liu, H.Y.; Wang, Y.; Han, T.L.; Huang, Q.S. Influence of vertex finder configurations on separation of fine particles. *CIESC J.* **2017**, *68*, 1921–1931. [CrossRef]
16. Hwang, I.S.; Jeong, H.J.; Hwang, J. Effects of vortex finder length on flow field and collection efficiency of cyclone in an industrial scale circulating fluidized bed boiler: Numerical study. *Int. J. Energy Res.* **2020**, *44*, 7229–7241. [CrossRef]
17. Tian, J.Y.; Ni, L.; Song, T.; Zhao, J.N. CFD simulation of hydrocyclone-separation performance influenced by reflux device and different vortex-finder lengths. *Sep. Purif. Technol.* **2019**, *233*, 116013. [CrossRef]

18. Noori, M.; Dehghan, R. Toward a better understanding of a Tri-Flo separator using prototyping, central composite design (CCD) and CFD simulation. *Int. J. Coal Prep. Util.* **2020**, *2*, 1–21. [CrossRef]
19. Xu, Y.X.; Tang, B.; Song, X.F.; Yu, J.G. A high-efficiency hydrocyclone designed by response surface methodology for acid hydrolysis residue recycling. *R. Soc. Open Sci.* **2019**, *6*, 172339. [CrossRef]
20. Zhang, Y.; Jiang, M.H.; Zhang, Y. The structure parameters optimization of co-rotating outflow hydrocyclone based on response surface methodology. *Chenmical Enginerr. Mach.* **2016**, *46*, 164–167.
21. Obeng, D.P.; Morrell, S. The JK three-product cyclone-performance and potential applications. *Int. J. Miner. Process.* **2003**, *69*, 129–142. [CrossRef]
22. Zhang, Y.K.; Liu, P.K.; Jiang, L.Y.; Yang, X.H.; Yang, J.R. Numerical Simulation of Flow Field Characteristics and Separation Performance Test of Multi-Product Hydrocyclone. *Minerals* **2019**, *9*, 300. [CrossRef]
23. Klavuz, F.S.; Gulsoy, O.Y. The effect of cone ratio on the separation efficiency of small diameter hydrocyclones. *Int. J. Miner. Process.* **2010**, *98*, 163–167. [CrossRef]
24. He, F.Q.; Zhang, Y.H.; Wang, J.G.; Yang, Q.; Tan, Y.H. Flow Patterns in Mini-Hydrocyclones with Different Vortex Finder Depths. *Chem. Eng. Technol.* **2013**, *6*, 1935–1942. [CrossRef]
25. Vieira, L.G.M.; Barrozo, M.A.S. Effect of vortex finder diameter on the performance of a novel hydrocyclone separator. *Miner. Eng.* **2014**, *57*, 50–56. [CrossRef]
26. Li, F.; Liu, P.K.; Yang, X.H.; Zhang, Y.K. Numerical simulation on the effects of different inlet pipe structures on the flow field and seperation performance in a hydrocyclone. *Powder Technol.* **2020**, *373*, 254–266. [CrossRef]
27. Wang, C.C.; Wu, R.M. Experimental and simulation of a novel hydrocyclone tubular membrane as overflow pipe. *Sep. Purif. Technol.* **2018**, *198*, 60–67. [CrossRef]
28. Kuang, S.B.; Chu, K.W.; Yu, A.B.; Vince, A. Numerical study of liquid–gas–solid flow in classifying hydrocyclones: Effect of feed solids concentration. *Miner. Eng.* **2012**, *31*, 17–31. [CrossRef]
29. Azimian, M.; Bart, H.J. Numerical analysis of hydroabrasion in a hydrocyclone. *Pet. Sci.* **2016**, *13*, 304–319. [CrossRef]
30. Gong, H.F.; Yu, B.; Dai, F.; Peng, Y.; Shao, J. Simulation on performance of a demulsification and dewatering device with coupling double fields: Swirl centrifugal field and high-voltage electric field. *Sep. Purif. Technol.* **2018**, *207*, 124–132. [CrossRef]
31. Ke, R.J.; Shingote, C.; Kadambi, J.R.; Furlan, J.; Visintainer, R. Experimental and Numerical Investigations of the Fluid Flow in a Hydroclyclone with an Air Core, Mining. *Metall. Explor.* **2020**, *37*, 277–286. [CrossRef]
32. Xu, X.; Ge, X.L.; Qian, Y.D.; Wang, H.L.; Yang, Q. Bubble-separation dynamics in a planar cyclone: Experiments and CFD simulations. *Aiche J.* **2018**, *64*, 2689–2701. [CrossRef]
33. Hsieh, K.T.; Rajamani, K. Phenomenological model of the hydrocyclone: Model development and verification for single-phase flow. *Int. J. Miner. Process.* **1988**, *22*, 223–237. [CrossRef]
34. Prashant, D.; Rachit, T.; Kumar, M.A.; Kumar, B.P. Application of response surface methodology for modeling and optimization of spiral separator for processing of iron ore slime. *Power Technol.* **2015**, *275*, 105–112. [CrossRef]
35. Sun, X.; Kim, S.; Yang, S.D.; Kim, H.S.; Yoon, J.Y. Multi-objective optimization of a Stairmand cyclone separator using response surface methodology and computational fluid dynamics. *Power Technol.* **2019**, *320*, 51–65. [CrossRef]
36. Ye, J.X.; Xu, Y.X.; Song, X.F.; Yu, J.G. Numerical modelling and multi-objective optimization of the novel hydrocyclone for ultra-fine particles classification. *Chem. Eng. Sci.* **2019**, *7*, 1072–1084. [CrossRef]
37. Jing, J.Q.; Zhang, S.J.; Qin, M.; Luo, J.Q.; Shan, Y.T.; Cheng, Y.Z.; Tan, J.T. Numerical simulation study of offshore heavy oil desanding by hydrocyclones. *Sep. Purif. Technol.* **2021**, *285*, 118051. [CrossRef]
38. Yu, J.F.; Fu, J.; Cheng, H.; Cui, Z.W. Recycling of rare earth particle by mini-hydrocyclones. *Waste Manag.* **2017**, *61*, 362–371. [CrossRef]